



# Manipulating Complex Hybrid Entanglement and Testing Multipartite Bell Inequalities in a Superconducting Circuit

Y. Ma,<sup>1</sup> X. Pan<sup>1</sup>,,<sup>1</sup> W. Cai,<sup>1</sup> X. Mu,<sup>1</sup> Y. Xu,<sup>1</sup> L. Hu,<sup>1</sup> W. Wang,<sup>1</sup> H. Wang,<sup>1</sup> Y. P. Song,<sup>1</sup>  
Zhen-Biao Yang,<sup>2,\*</sup> Shi-Biao Zheng,<sup>2,†</sup> and L. Sun<sup>1,‡</sup>

<sup>1</sup>Center for Quantum Information, Institute for Interdisciplinary Information Sciences, Tsinghua University, Beijing 100084, China

<sup>2</sup>Fujian Key Laboratory of Quantum Information and Quantum Optics, College of Physics and Information Engineering, Fuzhou University, Fuzhou, Fujian 350108, China



(Received 16 May 2020; accepted 23 September 2020; published 28 October 2020)

Quantum correlations in observables of multiple systems not only are of fundamental interest, but also play a key role in quantum information processing. As a signature of these correlations, the violation of Bell inequalities has not been demonstrated with multipartite hybrid entanglement involving both continuous and discrete variables. Here we create a five-partite entangled state with three superconducting transmon qubits and two photonic qubits, each encoded in the mesoscopic field of a microwave cavity. We reveal the quantum correlations among these distinct elements by joint Wigner tomography of the two cavity fields conditional on the detection of the qubits and by test of a five-partite Bell inequality. The measured Bell signal is  $8.381 \pm 0.038$ , surpassing the bound of 8 for a four-partite entanglement imposed by quantum correlations by 10 standard deviations, demonstrating the genuine five-partite entanglement in a hybrid quantum system.

DOI: [10.1103/PhysRevLett.125.180503](https://doi.org/10.1103/PhysRevLett.125.180503)

The ability of controllably entangling multiple quantum systems and individually detecting their states is of importance both from the fundamental viewpoint and for practical applications, e.g., quantum computation. Essentially, carrying out a quantum algorithm is physically equivalent to preparing and manipulating entanglement for many two-dimensional systems (qubits) in a prescribed manner, and then reading out their states [1,2]. Among various kinds of multipartite entangled states, the Greenberger-Horne-Zeilinger (GHZ) states represent a typical example [3], which have been produced in various systems [4–9]. These states are formed by two maximally distinct joint quantum states of three or more qubits, whose properties can exhibit strong quantum correlations that exclude any local realistic description of nature in an all-or-nothing manner [3] or by violation of multipartite Bell inequalities [10–12]. The ratio of the Bell's signal associated with a GHZ state to the bound allowed by local realism increases with the number of entangled qubits, indicating the larger the entanglement the stronger the nonclassical effect [12]. Besides fundamental interest, such states are a key resource for quantum-based technologies, including concatenated error correcting codes [13], quantum simulation [14,15], and Heisenberg-limited quantum metrology [16]. So far, experimental violations of multipartite Bell inequalities have been reported in photonic and trapped ion systems [17–19].

Circuit quantum electrodynamics (CQED) systems, with superconducting qubits coupled to resonators, are ideal for complex entanglement manipulation and quantum information processing [20–25]. Based on such systems, a

variety of entangled states have been produced, including multiphoton NOON states for two resonators [26,27], two-mode cat states for mesoscopic fields stored in two cavities [28], and multiqubit GHZ states [29–31]. Using entangled states of two superconducting qubits coupled to a resonator, violations of the Clauser-Horne-Shimony-Holt version of the Bell inequality have been demonstrated [32–34]. Recently, this violation was detected between two encoded cavity cat state qubits [28] and between a superconducting transmon qubit and an encoded cavity cat state qubit [35]; in these experiments, the Bell test was used to characterize two-partite entanglement other than to vindicate quantum nonlocality due to the lack of independent measurements of the two entangled constituents.

In this Letter we experimentally produce GHZ states for three superconducting transmon qubits and two encoded cavity cat qubits in a three-dimensional CQED architecture [36]. The entanglement among the three transmon qubits and the mesoscopic fields stored in the two cavities are generated by using the qubit-state-dependent cavity phase shifts and cavity-photon-number-dependent qubit rotations, enabled by the dispersive couplings between the cavities and the corresponding transmon qubits. As far as we know, this represents the largest hybrid entangled state reported so far; previously, hybrid entanglement was restricted to one discrete variable and two continuous variables [28]. We characterize the multipartite entanglement by measuring the joint Wigner functions for the two cavity fields conditional on outcomes of joint qubit detection and by testing the multipartite Bell inequality. We measure a Bell signal of

$8.381 \pm 0.038$ , surpassing the maximum value of 8 allowed by quantum mechanics for a four-partite quantum system. The results demonstrate a good control over complex three-dimensional CQED systems, which represent a promising platform for fault-tolerant quantum computation [37–40].

Our experiment is performed with a CQED architecture involving three superconducting transmon qubits, two storage cavities serving for storing photonic fields, and three readout cavities, each of which is dispersively coupled to one qubit for measuring the qubit state, as sketched in Fig. 1(a). The detailed device geometry can be found in Ref. [41] and the system parameters are listed in the Supplemental Material [42]. As the readout cavities remain in the vacuum state and do not affect the quantum state of the qubits and storage cavities during the entanglement production, we can ignore the state of each readout cavity and will refer to the corresponding storage cavity as “cavity.” Qubit  $Q_1$  ( $Q_2$ ) is dispersively coupled to cavity  $S_1$  ( $S_2$ ), while qubit  $Q_3$  is commonly coupled to both cavities. In the interaction picture, the Hamiltonian for the total system is

$$\begin{aligned}
 H_I = & -a_1^\dagger a_1 (\chi_{11}|e\rangle_1\langle e| + \chi_{13}|e\rangle_3\langle e|) \\
 & - a_2^\dagger a_2 (\chi_{22}|e\rangle_2\langle e| + \chi_{23}|e\rangle_3\langle e|), \quad (1)
 \end{aligned}$$

where  $a_j^\dagger$  and  $a_j$  are the creation and annihilation operators of the photonic field in cavity  $S_j$  ( $j = 1, 2$ ),  $|e\rangle_k$  denotes the excited state of qubit  $k$  ( $k = 1, 2, 3$ ), and  $\chi_{jk}$  is the frequency shift of cavity  $S_j$  conditional on the qubit state  $|e\rangle_k$  due to the dispersive coupling.

Based on the above Hamiltonian [Eq. (1)] and the conditional operations, we can generate a hybrid entangled state as in Fig. 1(b). Figure 1(c) shows the pulse sequence for the creation and the following characterization of this state. The experiment starts with initializing each qubit to the ground state  $|g\rangle$  and each cavity to vacuum state  $|0\rangle$ . After this initialization, we apply a microwave pulse to each cavity to produce a displacement operation  $D_j(\alpha_j)$  in phase space, translating the cavity from the vacuum state  $|0\rangle_j$  to a coherent state  $|\alpha_j\rangle_j$ , with  $\alpha_j$  being the complex amplitude of the phase-space displacement. The subsequent rotation  $R_y^{\pi/2}$  (a  $\pi/2$  rotation around the  $y$  axis) on qubit  $Q_3$ ,

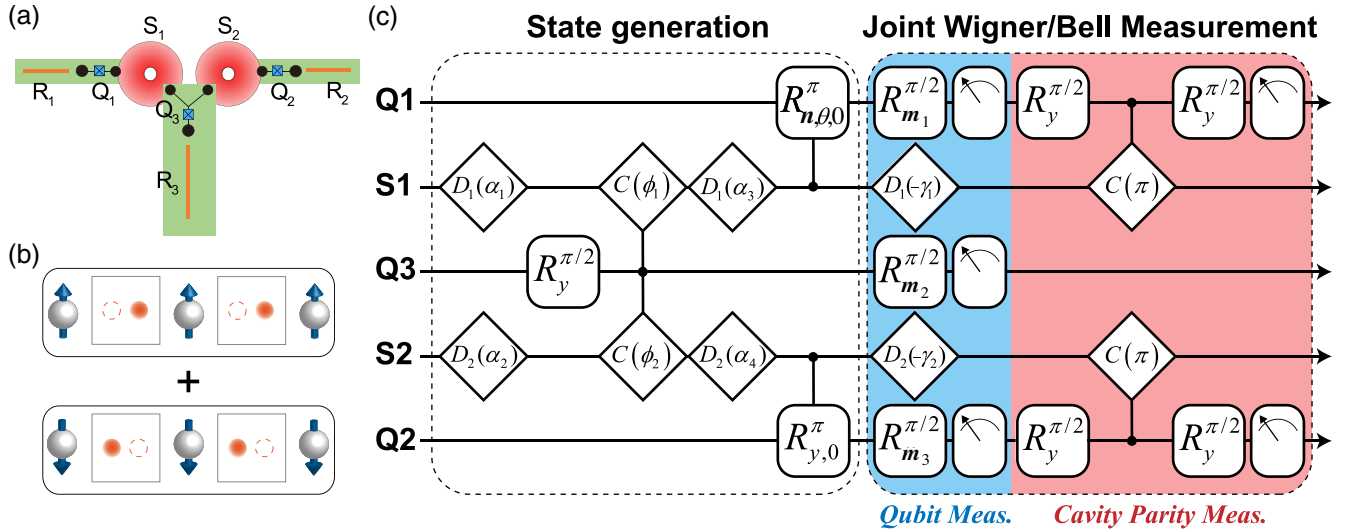


FIG. 1. Device sketch and pulse sequence. (a) Device sketch. The device involves three superconducting transmon qubits, labeled from  $Q_1$  to  $Q_3$ , with  $Q_1$  ( $Q_2$ ) dispersively coupled to the first (second) storage cavity, denoted as  $S_1$  ( $S_2$ ), and  $Q_3$  coupled to both storage cavities. Each qubit is independently coupled to a readout cavity. The storage cavities are used for storing the photonic fields, while the readout cavities for detecting the qubit states. (b) Schematic of hybrid entanglement containing three discrete variables and two continuous variables. (c) Experimental pulse sequence to create and characterize the entangled state in (b). The procedure consists of three parts. (1) Generation of the multipartite entangled state for the three transmon qubits and the two storage cavities, realized by a sequence of operations, including initialization of the system to the ground state, a pair of phase-space displacements  $D_1(\alpha_1 = 1.782)$  and  $D_2(\alpha_2 = 1.782)$  on the two cavity fields, rotation  $R_y^{\pi/2}$  of  $Q_3$ ,  $Q_3$ -state-dependent cavity phase shifts, a second pair of cavities displacements  $D_1(\alpha_3)$  and  $D_2(\alpha_4)$ , and  $\pi$  rotations  $R_{\mathbf{n},\theta,0}^\pi$  and  $R_{y,0}^\pi$  to  $Q_1$  and  $Q_2$  conditional on the vacuum states of  $S_1$  and  $S_2$ , respectively. The angle ( $\theta$ ) between the rotation axis of  $R_{\mathbf{n},\theta,0}^\pi$  and the  $\mathbf{n}$  axis is variable. (2) Measurement of the qubit observables with the appropriate  $\pi/2$  prerotations around the  $\mathbf{m}$  axis on the equatorial plane  $R_{\mathbf{m},j}^{\pi/2}$ , before the state readout in the basis  $\{|g_j\rangle, |e_j\rangle\}$ .  $R_{\mathbf{m},j}^{\pi/2} = R_{-y}^{\pi/2}$  for the joint Wigner measurement and  $R_{\mathbf{m},j}^{\pi/2} = R_{-y}^{\pi/2}$  or  $R_{\pm x}^{\pi/2}$  for the Bell signal measurement. (3) Displaced photon-number parity detection for each cavity, realized by performing a phase-space displacement  $D_j(-\gamma_j)$  and then sandwiching a conditional cavity  $\pi$ -phase shift between two qubit rotations  $R_y^{\pi/2}$  on the corresponding qubit.  $D_j(-\gamma_j)$  is used for conditional Wigner tomography and for  $\sigma_x$  measurement of the corresponding cavity cat state qubit. For  $\sigma_y$  measurement of each cavity, the displacement  $D_j(-\gamma_j)$  is replaced by the combination of two perpendicular displacements (see the main text).

achieved by the application of a driving pulse, transforms  $|g\rangle_3$  to  $(|g\rangle_3 + |e\rangle_3)/\sqrt{2}$ . After an interaction time  $\tau$ , the dispersive interaction of qubit  $Q_3$  with each cavity leads to a conditional phase shift [28,35,48–50], evolving the system to the state

$$|g\rangle_1|g\rangle_2(|g\rangle_3|\alpha_1\rangle_1|\alpha_2\rangle_2 + |e\rangle_3|\alpha_1 e^{i\phi_1}\rangle_1|\alpha_2 e^{i\phi_2}\rangle_2)/\sqrt{2}, \quad (2)$$

where  $\phi_j = \chi_{j3}\tau$ . A second displacement operation,  $D_1(\alpha_3 = -\alpha_1)$ , is then applied to cavity  $S_1$ , and  $D_2(\alpha_4 = -\alpha_2 e^{i\phi_2})$  to cavity  $S_2$ , resulting in the state

$$\frac{1}{\sqrt{2}}|g\rangle_1|g\rangle_2(e^{-i|\alpha_2|^2 \sin \phi_2}|g\rangle_3|0\rangle_1|\alpha_2 - \alpha_2 e^{i\phi_2}\rangle_2 + e^{i|\alpha_1|^2 \sin \phi_1}|e\rangle_3|\alpha_1 e^{i\phi_1} - \alpha_1\rangle_1|0\rangle_2). \quad (3)$$

After this operation, we perform a  $\pi$  rotation to each qubit conditional on the vacuum state of the corresponding cavity [26,48,50], realized by a pulse resonant with the qubit transition associated with the cavity's vacuum state  $|0\rangle$ . The conditional  $\pi$  rotation on  $Q_1$ , denoted as  $R_{\mathbf{n},\theta,0}^\pi$ , is around an axis with an adjustable angle  $\theta$  relative to the  $\mathbf{n}$  axis (reference axis) which has an angle  $\pi/2 + |\alpha_1|^2 \sin \phi_1 + |\alpha_2|^2 \sin \phi_2$  to the  $x$  axis on the equatorial plane, while that on  $Q_2$  ( $R_{\mathbf{y},0}^\pi$ ) is around the  $y$  axis. After these conditional rotations, the total system evolves to

$$(|e\rangle_1|g\rangle_2|g\rangle_3|0\rangle_1|\beta_2\rangle_2 + e^{-i\theta}|g\rangle_1|e\rangle_2|e\rangle_3|\beta_1\rangle_1|0\rangle_2)/\sqrt{2}, \quad (4)$$

where  $\beta_1 = (\alpha_1 e^{i\phi_1} - \alpha_1) e^{i\chi_{13}\tau}$  and  $\beta_2 = \alpha_2 - \alpha_2 e^{i\phi_2}$ , with  $\tau$  being the duration of these conditional rotations. When  $|\beta_j|^2 \gg 1$ ,  $|\beta_j\rangle_j$  and  $|0\rangle_j$  are approximately orthogonal and can be considered as the two logic states of a qubit. With this encoding, the state of Eq. (4) represents a five-partite GHZ state involving three transmon qubits and two cavity cat state qubits. In our experiment,  $\beta_1 = -2.7 - 0.2i$  and  $\beta_2 = 0.8 + 2.3i$ , corresponding to  $|\langle \beta_1 | 0 \rangle_1|^2 \simeq 6.6 \times 10^{-4}$  and  $|\langle \beta_2 | 0 \rangle_2|^2 \simeq 2.5 \times 10^{-3}$ .

To verify the entanglement among the transmon qubits and the cavity fields after the GHZ state generation, we measure the conditional two-mode Wigner functions  $W_1(\gamma_1, \gamma_2)$  and  $W_{-1}(\gamma_1, \gamma_2)$  [see Fig. 1(c)], which are defined as the joint Wigner functions for the two cavity fields conditional on  $X_1 X_2 X_3 = 1$  and  $-1$ , respectively. Here  $X_1 X_2 X_3$  represents the value of the observable  $\sigma_x^1 \sigma_x^2 \sigma_x^3$ , with  $\sigma_x^j$  being the  $x$  component of the Pauli operator associated with the  $j$ th transmon qubit. The observable  $\sigma_x^k$  is measured by performing the rotation  $R_{-y}^{\pi/2}$  on the  $k$ th qubit and then reading out its state in the basis  $\{|g\rangle_k, |e\rangle_k\}$ ; the outcomes  $|g\rangle_k$  and  $|e\rangle_k$  correspond to  $X_k = 1$  and  $-1$ , respectively. After the measurement of  $X_1$  ( $X_2$ ), transmon qubit  $Q_1$  ( $Q_2$ ) is used to measure the displaced photon-number parity of cavity  $S_1$  ( $S_2$ ), achieved by sandwiching a conditional cavity  $\pi$ -phase shift between two qubit rotations  $R_y^{\pi/2}$  after the corresponding

cavity displacement [28,35,48–52]. The joint displaced photon-number parity of two cavity fields is directly related with the two-mode Wigner function as

$$W(\gamma_1, \gamma_2) = \frac{4}{\pi^2} \langle P_{1,\gamma_1} P_{2,\gamma_2} \rangle, \quad (5)$$

where  $P_{j,\gamma_j} = D_j(\gamma_j) P_j D_j^\dagger(\gamma_j)$ , with  $P_j$  denoting the photon-number parity operator for cavity  $S_j$ . The two-mode Wigner function is a function in a four-dimensional space spanned by  $\{\text{Re}(\gamma_1), \text{Re}(\gamma_2), \text{Im}(\gamma_1), \text{Im}(\gamma_2)\}$ . We measure  $W(\gamma_1, \gamma_2)$  for both  $X_1 X_2 X_3 = 1$  and  $-1$ .

The two-dimensional plane-cuts of the measured conditional Wigner function  $W_1(\gamma_1, \gamma_2)$  and the ideal results are displayed in Figs. 2(a) and 2(b), respectively, while those associated with  $W_{-1}(\gamma_1, \gamma_2)$  are shown in Figs. 2(c) and 2(d). Here the relative phase between the two components

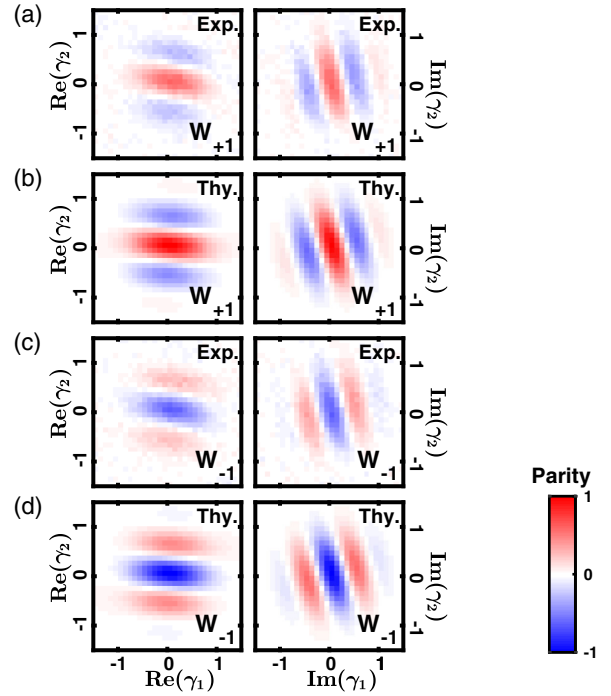


FIG. 2. Conditional two-mode Wigner tomography for  $S_1$  and  $S_2$  after generation of the GHZ state of Eq. (4) with  $\theta = 0$ . Two-dimensional plane-cuts along the  $\text{Re}(\gamma_1)$ - $\text{Re}(\gamma_2)$  axes with  $\text{Im}(\gamma_j) = 0$  and along the  $\text{Im}(\gamma_1)$ - $\text{Im}(\gamma_2)$  axes with  $\text{Re}(\gamma_j) = 0$  are shown in the left and right panels. We displace each mode with  $-\beta_1/2$  and  $-\beta_2/2$ , respectively, so that the center of the fringes is the origin. We note that the fringe direction relative to the horizontal axis is determined by  $\tan^{-1}[\text{Im}(\beta_1)/\text{Im}(\beta_2)]$  and  $\tan^{-1}[\text{Re}(\beta_1)/\text{Re}(\beta_2)]$  for the left and right panels respectively. (a) Cuts of the measured conditional Wigner function,  $W_1(\gamma_1, \gamma_2)$ , defined as the joint Wigner functions for the two cavity fields conditional on  $X_1 X_2 X_3 = 1$ . (b) The expected  $W_1(\gamma_1, \gamma_2)$ , calculated from the ideal state of Eq. (4) with  $\beta_1 = -2.7 - 0.2i$  and  $\beta_2 = 0.8 + 2.3i$ . (c) Cuts of the measured  $W_{-1}(\gamma_1, \gamma_2)$  conditional on  $X_1 X_2 X_3 = -1$ . (d) The expected  $W_{-1}(\gamma_1, \gamma_2)$ , also calculated from the ideal state as (a).

of the produced GHZ state is  $\theta = 0$ . Cuts along the  $\text{Re}(\gamma_1)\text{-Re}(\gamma_2)$  axes and  $\text{Im}(\gamma_1)\text{-Im}(\gamma_2)$  axes are shown in the left and right panels, respectively. As expected, both  $W_1(\gamma_1, \gamma_2)$  and  $W_{-1}(\gamma_1, \gamma_2)$  exhibit strong two-mode quantum interference features, evidenced by the fringes on the  $\text{Re}(\gamma_1)\text{-Re}(\gamma_2)$  and  $\text{Im}(\gamma_1)\text{-Im}(\gamma_2)$  planes [28,53]. The complementarity between the interference patterns of  $W_1(\gamma_1, \gamma_2)$  and  $W_{-1}(\gamma_1, \gamma_2)$  reveals the entanglement between the transmon qubits and the cavity fields.

The five-partite entanglement can be further revealed by the multipartite Bell inequality, proposed by Mermin [12]. For clarity, we rewrite this state as

$$(|\uparrow\rangle_1|\uparrow\rangle_2|\uparrow\rangle_3|\uparrow\rangle_4|\uparrow\rangle_5 + |\downarrow\rangle_1|\downarrow\rangle_2|\downarrow\rangle_3|\downarrow\rangle_4|\downarrow\rangle_5)/\sqrt{2}, \quad (6)$$

where  $|\uparrow\rangle_1 \equiv |e\rangle_1$  and  $|\downarrow\rangle_1 \equiv |g\rangle_1$ ;  $|\uparrow\rangle_k \equiv |g\rangle_k$  and  $|\downarrow\rangle_k \equiv |e\rangle_k$  for  $k = 2, 3$ ;  $|\uparrow\rangle_4 \equiv |0\rangle_1$  and  $|\downarrow\rangle_4 \equiv |\beta_1\rangle_1$ ;  $|\uparrow\rangle_5 \equiv |\beta_2\rangle_2$ ,  $|\downarrow\rangle_5 \equiv |0\rangle_2$ . The Bell operator for this hybrid system is defined as

$$\begin{aligned} \mathcal{B} = & \sigma_x^1 \sigma_x^2 \sigma_x^3 \sigma_x^4 \sigma_x^5 - \sum_l P_l (\sigma_x^1 \sigma_x^2 \sigma_x^3 \sigma_y^4 \sigma_y^5) \\ & + \sum_l P_l (\sigma_x^1 \sigma_y^2 \sigma_y^3 \sigma_y^4 \sigma_y^5), \end{aligned} \quad (7)$$

where  $\{P_l\}$  denotes the set of all distinct permutations of the subscripts that give distinct products. The measurement sequence is also shown in Fig. 1(c). As has been shown, for  $k \leq 3$  the observables  $\sigma_x^k$  are measured by performing the rotation  $R_{-y}^{\pi/2}$  before state readout of the corresponding qubit.  $\sigma_y^1$  is measured by performing the rotation  $R_{-x}^{\pi/2}$  before the state readout; for the measurement of  $\sigma_y^2$  and  $\sigma_y^3$ ,  $R_{-x}^{\pi/2}$  is replaced by  $R_x^{\pi/2}$ . For each of these measurements, the value of 1 (−1) is assigned to the corresponding observable when the outcome is  $|g\rangle_k$  ( $|e\rangle_k$ ). On the other hand, for  $k = 4$  and 5,  $\sigma_x^k$  and  $\sigma_y^k$  are measured by mapping them to displaced photon-number parity observables of the  $j$ th cavity with  $j = k - 3$  [35]:  $\sigma_x^k$  corresponds to  $P_{j,x} = D_j(\beta_j/2)P_j D_j(-\beta_j/2)$ ; while  $\sigma_y^k$  approximates  $P_{j,y} = D_j(\beta_j/2)D_j(-i\epsilon_j\pi/4\beta_j^*)P_j D_j(i\epsilon_j\pi/4\beta_j^*)D_j(-\beta_j/2)$ , where  $\epsilon_j = -1$  and 1 for  $j = 1$  and 2, respectively. The even and odd parities of the  $j$ th cavity after the corresponding displacement operation correspond to the values 1 and −1 for  $X_{j+3}$  or  $Y_{j+3}$ , respectively. The Bell operator involves 16 terms. The experiment is repeated 10 000 times for the measurement of the correlation corresponding to each term, which is obtained by averaging over all of the experimental outcomes. All the correlation values are combined to obtain the corresponding Bell signal according to the expansion of Eq. (7).

An ideal five-qubit GHZ state is the eigenstate of each term of  $\mathcal{B}$  with the eigenvalue 1, so that the ideal value of  $\langle \mathcal{B} \rangle$  is 16. The measured expectation value of the Bell operator,  $\langle \mathcal{B} \rangle$ , as a function of the relative phase ( $\theta$ ) of the

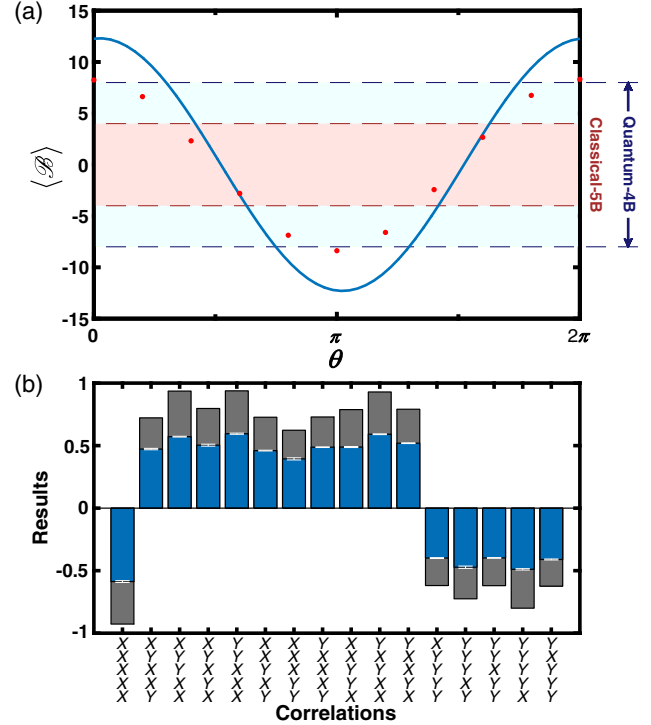


FIG. 3. Bell signal measurement. (a) Measured expectation value of the Bell operator  $\langle \mathcal{B} \rangle$  as a function of the relative phase ( $\theta$ ) of the produced GHZ state. An oscillation is observed as predicted. Experiment data are marked with red. Their standard deviations are obtained from ten repeated measurements when the system is stable and are smaller than marker sizes. Simulated results based on qutip in Python [54,55] are shown as the blue curve. In the simulation, we neglect the system decoherence in the GHZ state generation and calculate the expectation value of the Bell operator of Eq. (7) with thus obtained GHZ state. The maximum of the measured Bell signals  $|\langle \mathcal{B} \rangle| = 8.381 \pm 0.038$  not only exceeds the bound of 4 allowed by local realism (red region), but also above the bound of 8 for a four-partite entangled quantum system (light blue region), demonstrating the genuine five-partite entanglement in a hybrid system. (b) Correlations combining the maximum of the measured Bell signals in (a). Blue bars are experimental data and grey ones represent simulated results. Error bars are from repeated measurements. The measured results are lower due to the imperfections in the experiment (see the main text), but the overall distribution is consistent with simulation.

produced GHZ state is shown in Fig. 3(a). Because of the large Hilbert space spanned by this five-partite hybrid system, exact numerical simulations are difficult. Hence, we simplify the simulation by neglecting the system decoherence in the GHZ state generation and calculating the expectation value of the Bell operator of Eq. (7) with the simulated GHZ state. The simulated result is shown as the solid line. The correlation associated with each term of  $\mathcal{B}$  at the maximum ( $\theta = \pi$ ) is plotted in Fig. 3(b). Blue bars are experimental data and grey ones correspond to the simulated results.



The simulated correlations deviate from 1 and give the maximum value of Bell signal of only  $|\langle \mathcal{B} \rangle| = 12.29$ . This is mainly due to the following two factors. The first one is the Kerr effects which deform the coherent state components of the cavities and cause an imperfection of the conditional qubit rotations, but are not included in the Hamiltonian of Eq. (1). The second one is the limitation of the displacement  $\beta_j$ , which leads to a discrepancy between the displaced parity operator  $P_{j,y}$  for the  $j$ th cavity and the  $y$  component of the Pauli operator for the  $k$ th qubit (see Supplemental Material [42]).

The measured values are even lower because of (1) the qubit decoherence and cavity photon losses during the state generation and the following characterization; (2) the large cavity field amplitudes that cause the parity measurement following the displacements  $D_j(-\gamma_j)$  to deviate from the expected cavity observables; (3) the readout errors of the qubit states, to which the Bell signal is very sensitive. This is due to the fact that once a qubit readout error occurs, the sign of the output value of the corresponding measured term is changed. Nevertheless, the resulting measured Bell signal is  $|\langle \mathcal{B} \rangle| = 8.381 \pm 0.038$  at the maximum, in good agreement with expectation after considering the above imperfections (Supplemental Material [42]). This value not only exceeds the bound of 4 allowed by local realism [12], but also is above the bound of 8 for a four-partite entangled quantum system, demonstrating the genuine five-partite entanglement in a hybrid system.

We have experimentally demonstrated controlled entanglement manipulation and characterization in a CQED quantum processor involving three superconducting transmon qubits and two cavities storing mesoscopic fields. We deterministically entangled all these elements and verified their quantum correlations by reconstructing the joint Wigner functions of the two cavities conditional on the detection of the states of the qubits. We further measure the five-partite Bell signal of  $8.381 \pm 0.038$ , exceeding the maximum value of 8 for a four-partite entangled state by 10 standard deviations. Apart from fundamental interest, our experiment serves as a demonstration of good control over a quantum circuit, which is important for solid-state quantum computation. For larger systems with qubit-cavity chain geometry, the multipartite GHZ states can be prepared in a sequential way based on the same scheme presented in this work.

This work was supported by the National Natural Science Foundation of China under Grants No. 11674060, No. 11874114, No. 11874235, No. 11875108, and No. 11925404, National Key Research and Development Program of China under Grant No. 2017YFA0304303, and the Natural Science Foundation of Fujian Province under Grant No. 2018J01412.

Y. M. and X. P. contributed equally to this work.

\*zbyang@fzu.edu.cn

†t96034@fzu.edu.cn

‡luyansun@tsinghua.edu.cn

- [1] M. A. Nielsen and I. L. Chuang, *Quantum Computation and Quantum Information* (Cambridge University Press, Cambridge, England, 2000).
- [2] R. Raussendorf and H. J. Briegel, A One-Way Quantum Computer, *Phys. Rev. Lett.* **86**, 5188 (2001).
- [3] D. M. Greenberger, M. A. Horne, A. Shimony, and A. Zeilinger, Bell's theorem without inequalities, *Am. J. Phys.* **58**, 1131 (1990).
- [4] P. Neumann, N. Mizuochi, F. Rempp, P. Hemmer, H. Watanabe, S. Yamasaki, V. Jacques, T. Gaebel, F. Jelezko, and J. Wrachtrup, Multipartite entanglement among single spins in diamond, *Science* **320**, 1326 (2008).
- [5] M. Neeley, R. C. Bialczak, M. Lenander, E. Lucero, M. Mariantoni, A. D. O'Connell, D. Sank, H. Wang, M. Weides, J. Wenner, Y. Yin, T. Yamamoto, A. N. Cleland, and J. M. Martinis, Generation of three-qubit entangled states using superconducting phase qubits, *Nature (London)* **467**, 570 (2010).
- [6] L. Dicarlo, M. D. Reed, L. Sun, B. R. Johnson, J. M. Chow, J. M. Gambetta, L. Frunzio, S. M. Girvin, M. H. Devoret, and R. J. Schoelkopf, Preparation and measurement of three-qubit entanglement in a superconducting circuit, *Nature (London)* **467**, 574 (2010).
- [7] R. Barends, J. Kelly, A. Megrant, A. Veitia, D. Sank, E. Jeffrey, T. C. White, J. Mutus, A. G. Fowler, B. Campbell, Y. Chen, Z. Chen, B. Chiaro, A. Dunsworth, C. Neill, P. O'Malley, P. Roushan, A. Vainsencher, J. Wenner, A. N. Korotkov, A. N. Cleland, and J. M. Martinis, Superconducting quantum circuits at the surface code threshold for fault tolerance, *Nature (London)* **508**, 500 (2014).
- [8] X.-L. Wang, L.-K. Chen, W. Li, H.-L. Huang, C. Liu, C. Chen, Y.-H. Luo, Z.-E. Su, D. Wu, Z.-D. Li, H. Lu, Y. Hu, X. Jiang, C.-Z. Peng, L. Li, N.-L. Liu, Y.-A. Chen, C.-Y. Lu, and J.-W. Pan, Experimental Ten-Photon Entanglement, *Phys. Rev. Lett.* **117**, 210502 (2016).
- [9] T. Monz, P. Schindler, J. T. Barreiro, M. Chwalla, D. Nigg, W. A. Coish, M. Harlander, W. Hänsel, M. Hennrich, and R. Blatt, 14-Qubit Entanglement: Creation and Coherence, *Phys. Rev. Lett.* **106**, 130506 (2011).
- [10] J. S. Bell, On the Einstein-Podolsky-Rosen paradox, *Physics (Long Island City, NY)* **1**, 195 (1965).
- [11] J. F. Clauser, M. A. Horne, A. Shimony, and R. A. Holt, Proposed Experiment to Test Local Hidden-Variable Theories, *Phys. Rev. Lett.* **23**, 880 (1969).
- [12] N. D. Mermin, Extreme Quantum Entanglement in a Superposition of Macroscopically Distinct States, *Phys. Rev. Lett.* **65**, 1838 (1990).
- [13] E. Knill, Quantum computing with realistically noisy devices, *Nature (London)* **434**, 39 (2005).
- [14] Y. P. Zhong, D. Xu, P. Wang, C. Song, Q. J. Guo, W. X. Liu, K. Xu, B. X. Xia, C.-Y. Lu, S. Han, J. W. Pan, and H. Wang, Emulating Anyonic Fractional Statistical Behavior in a Superconducting Quantum Circuit, *Phys. Rev. Lett.* **117**, 110501 (2016).

- [15] C. Song, D. Xu, P. Zhang, J. Wang, Q. Guo, W. Liu, K. Xu, H. Deng, K. Huang, D. Zheng, S.-B. Zheng, H. Wang, X. Zhu, C.-Y. Lu, and J.-W. Pan, Demonstration of Topological Robustness of Anyonic Braiding Statistics with a Superconducting Quantum Circuit, *Phys. Rev. Lett.* **121**, 030502 (2018).
- [16] D. Leibfried, M. D. Barrett, T. Schaetz, J. Britton, J. Chiaverini, W. M. Itano, J. D. Jost, C. Langer, and D. J. Wineland, Toward Heisenberg-limited spectroscopy with multiparticle entangled states, *Science* **304**, 1476 (2004).
- [17] B. P. Lanyon, M. Zwerger, P. Jurcevic, C. Hempel, W. Dür, H. J. Briegel, R. Blatt, and C. F. Roos, Experimental Violation of Multipartite Bell Inequalities with Trapped Ions, *Phys. Rev. Lett.* **112**, 100403 (2014).
- [18] P. Walther, M. Aspelmeyer, K. J. Resch, and A. Zeilinger, Experimental Violation of a Cluster State Bell Inequality, *Phys. Rev. Lett.* **95**, 020403 (2005).
- [19] W.-B. Gao, X.-C. Yao, P. Xu, H. Lu, O. Gühne, A. Cabello, C.-Y. Lu, T. Yang, Z.-B. Chen, and J.-W. Pan, Bell inequality tests of four-photon six-qubit graph states, *Phys. Rev. A* **82**, 042334 (2010).
- [20] J. Q. You and F. Nori, Quantum information processing with superconducting qubits in a microwave field, *Phys. Rev. B* **68**, 064509 (2003).
- [21] A. Blais, R.-S. Huang, A. Wallraff, S. M. Girvin, and R. J. Schoelkopf, Cavity quantum electrodynamics for superconducting electrical circuits: An architecture for quantum computation, *Phys. Rev. A* **69**, 062320 (2004).
- [22] A. Wallraff, D. I. Schuster, A. Blais, L. Frunzio, R.-S. Huang, J. Majer, S. Kumar, S. M. Girvin, and R. J. Schoelkopf, Strong coupling of a single photon to a superconducting qubit using circuit quantum electrodynamics, *Nature (London)* **431**, 162 (2004).
- [23] J. Q. You and F. Nori, Atomic physics and quantum optics using superconducting circuits, *Nature (London)* **474**, 589 (2011).
- [24] M. H. Devoret and R. J. Schoelkopf, Superconducting circuits for quantum information: An outlook, *Science* **339**, 1169 (2013).
- [25] X. Gu, A. F. Kockum, A. Miranowicz, Y. X. Liu, and F. Nori, Microwave photonics with superconducting quantum circuits, *Phys. Rep.* **718–719**, 1 (2017).
- [26] H. Wang, M. Mariantoni, R. C. Bialczak, M. Lenander, E. Lucero, M. Neeley, A. D. O’Connell, D. Sank, M. Weides, J. Wenner, T. Yamamoto, Y. Yin, J. Zhao, J. M. Martinis, and A. N. Cleland, Deterministic Entanglement of Photons in Two Superconducting Microwave Resonators, *Phys. Rev. Lett.* **106**, 060401 (2011).
- [27] Y. Y. Gao, B. J. Lester, K. S. Chou, L. Frunzio, M. H. Devoret, L. Jiang, S. M. Girvin, and R. J. Schoelkopf, Entanglement of bosonic modes through an engineered exchange interaction, *Nature (London)* **566**, 509 (2019).
- [28] C. Wang, Y. Y. Gao, P. Reinhold, R. W. Heeres, N. Ofek, K. Chou, C. Axline, M. Reagor, J. Blumoff, K. M. Sliwa, L. Frunzio, S. M. Girvin, L. Jiang, M. Mirrahimi, M. H. Devoret, and R. J. Schoelkopf, A Schrödinger cat living in two boxes, *Science* **352**, 1087 (2016).
- [29] H. Paik, A. Mezzacapo, M. Sandberg, D. T. McClure, B. Abdo, A. D. Córcoles, O. Dial, D. F. Bogorin, B. L. T. Plourde, M. Steffen, A. W. Cross, J. M. Gambetta, and J. M. Chow, Experimental Demonstration of a Resonator-Induced Phase Gate in a Multiqubit Circuit-QED System, *Phys. Rev. Lett.* **117**, 250502 (2016).
- [30] C. Song, K. Xu, W. Liu, C.-p. Yang, S.-B. Zheng, H. Deng, Q. Xie, K. Huang, Q. Guo, L. Zhang, P. Zhang, D. Xu, D. Zheng, X. Zhu, H. Wang, Y.-A. Chen, C.-Y. Lu, S. Han, and J.-W. Pan, 10-Qubit Entanglement and Parallel Logic Operations with a Superconducting Circuit, *Phys. Rev. Lett.* **119**, 180511 (2017).
- [31] C. Song, K. Xu, H. Li, Y.-R. Zhang, X. Zhang, W. Liu, Q. Guo, Z. Wang, W. Ren, J. Hao, H. Feng, H. Fan, D. Zheng, D.-W. Wang, H. Wang, and S.-Y. Zhu, Generation of multicomponent atomic Schrödinger cat states of up to 20 qubits, *Science* **365**, 574 (2019).
- [32] M. Ansmann, H. Wang, R. C. Bialczak, M. Hofheinz, E. Lucero, M. Neeley, A. D. O’Connell, D. Sank, M. Weides, J. Wenner, A. N. Cleland, and J. M. Martinis, Violation of Bell’s inequality in Josephson phase qubits, *Nature (London)* **461**, 504 (2009).
- [33] J. M. Chow, L. DiCarlo, J. M. Gambetta, A. Nunnenkamp, L. S. Bishop, L. Frunzio, M. H. Devoret, S. M. Girvin, and R. J. Schoelkopf, Detecting highly entangled states with a joint qubit readout, *Phys. Rev. A* **81**, 062325 (2010).
- [34] Y. P. Zhong, H.-S. Chang, K. J. Satzinger, M.-H. Chou, A. Bienfait, C. R. Conner, E. Dumur, J. Grebel, G. A. Peairs, R. G. Povey, D. I. Schuster, and A. N. Cleland, Violating Bell’s inequality with remotely connected superconducting qubits, *Nat. Phys.* **15**, 741 (2019).
- [35] B. Vlastakis, A. Petrenko, N. Ofek, L. Sun, Z. Leghtas, K. Sliwa, Y. Liu, M. Hatridge, J. Blumoff, L. Frunzio, M. Mirrahimi, L. Jiang, M. H. Devoret, and R. J. Schoelkopf, Characterizing entanglement of an artificial atom and a cavity cat state with Bell’s inequality, *Nat. Commun.* **6**, 8970 (2015).
- [36] H. Paik, D. I. Schuster, L. S. Bishop, G. Kirchmair, G. Catelani, A. P. Sears, B. R. Johnson, M. J. Reagor, L. Frunzio, L. I. Glazman, S. M. Girvin, M. H. Devoret, and R. J. Schoelkopf, Observation of High Coherence in Josephson Junction Qubits Measured in a Three-Dimensional Circuit QED Architecture, *Phys. Rev. Lett.* **107**, 240501 (2011).
- [37] N. Ofek, A. Petrenko, R. Heeres, P. Reinhold, Z. Leghtas, B. Vlastakis, Y. Liu, L. Frunzio, S. M. Girvin, L. Jiang, M. Mirrahimi, M. H. Devoret, and R. J. Schoelkopf, Extending the lifetime of a quantum bit with error correction in superconducting circuits, *Nature (London)* **536**, 441 (2016).
- [38] L. Hu, Y. Ma, W. Cai, X. Mu, Y. Xu, W. Wang, Y. Wu, H. Wang, Y. P. Song, C. L. Zou, S. M. Girvin, L. M. Duan, and L. Sun, Quantum error correction and universal gate set operation on a binomial bosonic logical qubit, *Nat. Phys.* **15**, 503 (2019).
- [39] P. Reinhold, S. Rosenblum, W.-L. Ma, L. Frunzio, L. Jiang, and R. J. Schoelkopf, Error-corrected gates on an encoded qubit, *Nat. Phys.* **16**, 822 (2020).
- [40] Y. Ma, Y. Xu, X. Mu, W. Cai, L. Hu, W. Wang, X. Pan, H. Wang, Y. P. Song, C. L. Zou, and L. Sun, Error-transparent operations on a logical qubit protected by quantum error correction, *Nat. Phys.* **16**, 827 (2020).

- [41] Y. Xu, Y. Ma, W. Cai, X. Mu, W. Dai, W. Wang, L. Hu, X. Li, J. Han, H. Wang, Y. P. Song, Z.-B. Yang, S.-B. Zheng, and L. Sun, Demonstration of Controlled-Phase Gates Between Two Error-Correctable Photonic Qubits, *Phys. Rev. Lett.* **124**, 120501 (2020).
- [42] See Supplemental Material at <http://link.aps.org/supplemental/10.1103/PhysRevLett.125.180503> for a discussion of upper bound of Bell signals for four-partite entanglement, displaced parity operators acting as  $y$  components of Pauli operators for cavity-encoded qubits, experimental device and parameters, measurement calibrations and estimation of measured Bell signal visibility, influence of biased measurements on the measured Bell signal, experimental sequences and numerical simulations, and qubit-state-dependent Wigner function, which include Refs. [40,41,43–48].
- [43] M. Reagor, W. Pfaff, C. Axline, R. W. Heeres, N. Ofek, K. Sliwa, E. Holland, C. Wang, J. Blumoff, K. Chou, M. J. Hatridge, L. Frunzio, M. H. Devoret, L. Jiang, and R. J. Schoelkopf, Quantum memory with millisecond coherence in circuit QED, *Phys. Rev. B* **94**, 014506 (2016).
- [44] C. Axline, M. Reagor, R. Heeres, P. Reinhold, C. Wang, K. Shain, W. Pfaff, Y. Chu, L. Frunzio, and R. J. Schoelkopf, An architecture for integrating planar and 3D cQED devices, *Appl. Phys. Lett.* **109**, 042601 (2016).
- [45] R. Vijay, M. H. Devoret, and I. Siddiqi, Invited review article: The Josephson bifurcation amplifier, *Rev. Sci. Instrum.* **80**, 111101 (2009).
- [46] N. Bergeal, F. Schackert, M. Metcalfe, R. Vijay, V. E. Manucharyan, L. Frunzio, D. E. Prober, R. J. Schoelkopf, S. M. Girvin, and M. H. Devoret, Phase-preserving amplification near the quantum limit with a Josephson ring modulator, *Nature (London)* **465**, 64 (2010).
- [47] W. Pfaff, C. J. Axline, L. D. Burkhardt, U. Vool, P. Reinhold, L. Frunzio, L. Jiang, M. H. Devoret, and R. J. Schoelkopf, Controlled release of multiphoton quantum states from a microwave cavity memory, *Nat. Phys.* **13**, 882 (2017).
- [48] B. Vlastakis, G. Kirchmair, Z. Leghtas, S. E. Nigg, L. Frunzio, S. M. Girvin, M. Mirrahimi, M. H. Devoret, and R. J. Schoelkopf, Deterministically encoding quantum information using 100-photon Schrödinger cat states, *Science* **342**, 607 (2013).
- [49] L. Sun, A. Petrenko, Z. Leghtas, B. Vlastakis, G. Kirchmair, K. M. Sliwa, A. Narla, M. Hatridge, S. Shankar, J. Blumoff, L. Frunzio, M. Mirrahimi, M. H. Devoret, and R. J. Schoelkopf, Tracking photon jumps with repeated quantum non-demolition parity measurements, *Nature (London)* **511**, 444 (2014).
- [50] K. Liu, Y. Xu, W. Wang, S.-B. Zheng, T. Roy, S. Kundu, M. Chand, A. Ranadive, R. Vijay, Y. Song, L. Duan, and L. Sun, A twofold quantum delayed-choice experiment in a superconducting circuit, *Sci. Adv.* **3**, e1603159 (2017).
- [51] W. Wang, L. Hu, Y. Xu, K. Liu, Y. Ma, S.-B. Zheng, R. Vijay, Y. P. Song, L.-M. Duan, and L. Sun, Converting Quasiclassical States into Arbitrary Fock State Superpositions in a Superconducting Circuit, *Phys. Rev. Lett.* **118**, 223604 (2017).
- [52] P. Bertet, A. Auffeves, P. Maioli, S. Osnaghi, T. Meunier, M. Brune, J. M. Raimond, and S. Haroche, Direct Measurement of the Wigner Function of a One-Photon Fock State in a Cavity, *Phys. Rev. Lett.* **89**, 200402 (2002).
- [53] P. Milman, A. Auffeves, F. Yamaguchi, M. Brune, J. M. Raimond, and S. Haroche, A proposal to test Bell's inequalities with mesoscopic non-local states in cavity QED, *Eur. Phys. J. D* **32**, 233 (2005).
- [54] J. R. Johansson, P. D. Nation, and F. Nori, QuTiP: An open-source python framework for the dynamics of open quantum systems, *Comput. Phys. Commun.* **183**, 1760 (2012).
- [55] J. R. Johansson, P. D. Nation, and F. Nori, QuTiP 2: A python framework for the dynamics of open quantum systems, *Comput. Phys. Commun.* **184**, 1234 (2013).